The developmental hourglass model is applicable to the spinal cord

Katsuki Mukaigasa*, Chie Sakuma, Hiroyuki Yaginuma

Department of Neuroanatomy and Embryology, School of Medicine, Fukushima Medical University

*Correspondence: kamukaig@fmu.ac.jp

Summary

The developmental hourglass model predicts that embryonic morphology is most conserved at the mid-embryonic stage and diverges at the early and late stages. This model is generally considered by whole embryonic level. Here, we demonstrate that the hourglass model is also applicable to a reduced element, the spinal cord. In the middle of spinal cord development, dorsoventrally arrayed neuronal progenitor domains are established, which are conserved among vertebrates. We found that, by comparing the single-cell transcriptomes between mice and zebrafish, V3 interneurons, a subpopulation of the post-mitotic spinal neurons, display divergent molecular profiles. We also found non-conservation of *cis*-regulatory elements located around the progenitor fate determinants, indicating the rewiring of the upstream gene regulatory network. These results demonstrate that, despite the conservation of the progenitor domains, processes before and after the progenitor domain specification diverged. This study may help understand the molecular basis of the developmental hourglass model.

Keywords

The developmental hourglass model, Single cell RNA-seq, *Cis* regulatory module, Gene regulatory network, Evolution, Spinal cord

Introduction

The vertebrate neural tube can produce a diverse array of neurons in a precisely controlled and reproducible manner. During neurogenesis and neuronal differentiation, each neuron is assigned a distinct feature, such as neurotransmitter phenotype, axonal projection pathway, and cell body localization (Lai et al., 2016; Lu et al., 2015; Sagner and Briscoe, 2019). The initial phase of this process is the fate specification of progenitor cells, whereby molecularly defined progenitor domains are established with sharp boundaries along the dorsoventral axis of the neural tube (Briscoe et al., 2000). Each progenitor identity is specified through a highly complex gene regulatory network (GRN), which is composed of graded Shh signaling activity localized ventrally, Bmp and Wnt signaling molecules expressed dorsally, pan-neural transcriptional activator Sox1–3, and a number of domain-specific transcription factors (TFs) functioning as repressors (Andrews et al., 2019; Balaskas et al., 2012; Delás and Briscoe, 2020; Kutejova et al., 2016; Nishi et al., 2015; Oosterveen et al., 2012; Peterson et al., 2012; Sagner and Briscoe, 2019; Zagorski et al., 2017). As the output of the GRN, 11 progenitor domains, termed dp1–6 in the dorsal half, and p0, p1, p2, pMN and p3 in the ventral half, are established (Lai et al., 2016; Lu et al., 2015; Sagner and Briscoe, 2019). Subsequently, multiple neuronal subtypes are generated from a single progenitor domain. For example, V2a, V2b and V2c interneurons (INs) are differentiated from the p2 domain (Del Barrio et al., 2007; Li et al., 2005; Panayi et al., 2010; Peng et al., 2007), and dI1i and dI1c INs are differentiated from the dp1 domain (Ding et al., 2012; Wilson et al., 2008). Each subtype of post-mitotic neurons proceeds to the maturation process, such as migration, axonal projection and circuit formation.

These knowledges have been constructed mainly based on the chick and mouse studies, while a number of studies using zebrafish have demonstrated that the spatial architecture of the progenitor domains in the neural tube is largely conserved among vertebrates (Cheesman and Eisen, 2004; Cheesman et al., 2004; Gribble et al., 2007; Guner and Karlstrom, 2007; Lewis et al., 2005; Park et al., 2002; Schäfer et al., 2005).

However, there exist overt differences between amniotes and teleosts with regard to post-mitotic neuronal maturation. For example, V2a INs, which are defined by the expression of Vsx2 (Chx10), contribute to the locomotor rhythm generation in zebrafish (Eklöf-Ljunggren et al., 2012), whereas V2a INs in mice play a role in the left-right alternation of limbs by providing excitatory input to the commissural INs (Crone et al., 2008, 2009). This implies that, during post-mitotic differentiation in mice and zebrafish, V2a INs are assigned different properties, or are placed in different positions within the spinal locomotor circuit (Kiehn, 2016). Another example is Robo3, an axon guidance receptor that is essential for commissural axons to cross the midline (Friocourt and Chédotal, 2017; Marillat et al., 2004; Sabatier et al., 2004). In the spinal cord of amniotes, Robo3 is expressed in V0, V1, and V3 INs in the ventral spinal cord, which encompass commissural INs (Friocourt et al., 2019; Tulloch et al., 2019). However, in zebrafish, although double labeling of *robo3* and neuronal subtype markers is not conducted, *robo3* expression is observed in the region encompassing MNs (Challa et al., 2005). If zebrafish MNs express *bona fide robo3*, the role of Robo3 has diverged between amniotes and zebrafish, as MNs of amniotes never express Robo3 (Friocourt et al., 2019; Tulloch et al., 2019).

In addition to the post-mitotic differentiation, a process before the establishment of progenitor domains also differs in amniotes and zebrafish. *Shh* is an essential gene for specification of the ventral neural tube, and is expressed in the notochord and floor plate in amniotes (Echelard et al., 1993; Riddle et al., 1993; Roelink et al., 1994). In contrast, 3 *Shh*-

74 related genes, *shha* (*sonic hedgehog*), *shhb* (*tiggy winkle hedgehog*) and *ihhb* (*echidna*
75 *hedgehog*) are expressed in notochord and/or floor plate in zebrafish, conferring a functional
76 redundancy of hedgehog (Hh) signaling (Currie and Ingham, 1996; Ekker et al., 1995; Krauss
77 et al., 1993). The Hh signaling pathway culminates in Gli family TFs, which function as
78 transcriptional activator or repressor depending on Hh signaling activity (Briscoe and Thérond,
79 2013). Amniotes possess three *Gli* genes (*Gli1*, *Gli2* and *Gli3*), whereas teleosts possess four
80 *Gli* genes (*gli1*, *gli2a*, *gli2b* and *gli3*). Loss of function experiments of *Gli* genes led to clearly
81 different phenotypes between mice and zebrafish. For example, *Gli1* knock-out mice are viable
82 and appear normal, showing that *Gli1* is not essential for embryogenesis in mice (Park et al.,
83 2000). In contrast, *gli1* mutant zebrafish displayed severe cranial motor neuron deficiency and
84 reduced Hh-target genes such as *ptch1* and *nkx2.2a*, and died at the larval stage (Chandrasekhar
85 et al., 1999; Karlstrom et al., 1996, 2003). In *Gli2* knock-out mice, the floor plate was not
86 specified, and MNs aberrantly occupied the ventral-most domain in the spinal cord, though
87 MN itself was differentiated (Ding et al., 1998; Matise et al., 1998), whereas in zebrafish, *gli2a*
88 is completely dispensable for normal embryogenesis and growth to adulthood (Karlstrom et
89 al., 2003; Vanderlaan et al., 2005; Wang et al., 2013), and *gli2b* knock-down caused a marked
90 reduction of MNs in the spinal cord (Ke et al., 2008). Knock-down of *gli3* in zebrafish led to
91 the reduction of MNs (Vanderlaan et al., 2005); however, in *Gli3* mutant mice, patterning
92 defects of the floor plate and MNs were not observed (Persson et al., 2002).

93 Overall, the processes before and after the progenitor domain specification have diverged
94 among vertebrates, despite the conservation of the dorsoventral arrangement of the progenitor
95 domains. This pattern of developmental divergence is highly consistent with the developmental
96 hourglass model, which argue that embryonic morphology at the early and late developmental
97 stages are divergent and that that at the mid-embryonic stage is conserved (Duboule, 1994; Hu
98 et al., 2017; Irie and Kuratani, 2014). However, the process of spinal cord development has

never been investigated from the perspective of this model. Here, we provide evidence supporting that the developmental hourglass model is applicable to spinal cord development. We examined the single-cell transcriptome data from mice and zebrafish, and provide another example of diverse differentiation of post-mitotic neurons. We also examined the transcriptional regulatory elements in the neural tube patterning genes based on ChIP-seq and ATAC-seq data, and sequence conservation, suggesting that GRN upstream to the progenitor domain specification has been rewired during vertebrate evolution. Based on our findings and robust development of the neuronal progenitor specification (Balaskas et al., 2012; Delás and Briscoe, 2020; Exelby et al., 2021; Xiong et al., 2013; Zagorski et al., 2017), we propose that the progenitor domain configuration in the neural tube is less evolvable due to its canalization (Waddington, 1942, 1957).

Results

Two distinct subtypes of V3 INs in amniotes

Neuronal subtypes repertoire of V3 INs, which are differentiated from ventral-most p3 progenitor domain, is relatively less studied among spinal neurons, both in amniotes and teleosts. Thus, we focused on V3 INs to clarify to what extent the post mitotic neuronal differentiation has diverged among vertebrates. We examined single-cell RNA-sequence (scRNA-seq) data obtained from the spinal cord of mouse embryos (Delile et al., 2019). The data consist of the whole spinal cord cells from embryonic day (E) 9.5 to E13.5. We extracted data with V3 IN profiles (*Nkx2-2* or *Sim1* positive), applied graph-based clustering and dimensionality reduction by tSNE to these cells, and then identified the differentially expressed genes in each cluster (Table S1). The expression levels of several markers were visualized on tSNE plots (Fig.1A). *Nkx2-2* is a marker of p3 progenitor domain and V3 INs (Briscoe et al., 1999). *Sim1* is a post-mitotic V3 IN marker (Zhang et al., 2008). V3 INs are glutamatergic

124 neurons, and thus express *Slc17a6* (*vGlut2*) (Zhang et al., 2008). Expression of *Sox2*, *Neurog3*
125 and *Tubb3* (*class III β-tubulin*) in this order indicates the transition from progenitor to
126 differentiated neuron (Carcagno et al., 2014). Thus, medial to lateral direction in the spinal
127 cord corresponds to top to bottom direction in this plot. We found at least two distinct
128 populations in V3 INs; one positive for *Robo3*, *Olig3*, and *Cntn2* (*Tag1*) (Cluster 5 in Fig.1A),
129 and the other positive for *Lhx1* (Cluster 1 in Fig.1A, Table S1).

130 To distinguish these two subtypes *in vivo*, markers of each subtype (*ROBO3* and LHX1)
131 were examined in the spinal cord of the chick embryo at Hamburger-Hamilton (HH) stage 25–
132 26 (Fig.1B–K). NKX2-2 was used as a marker of the p3 progenitor domain and V3 INs. Post-
133 mitotic V3 INs were distinguished by the expression of *SIM1*. We found that the expression of
134 *ROBO3* was localized medially within post-mitotic V3 INs. To confirm this further,
135 commissural axons passing through and bisecting the V3 INs were utilized as landmarks. Some
136 V3 INs were observed laterally to the commissural axons; however, these cells did not express
137 *ROBO3* (Fig.1F, G, K). Rather, *ROBO3* was expressed selectively by V3 INs located medially
138 to the commissural axons (Fig.1F, G). In contrast, LHX1 was expressed in the laterally located
139 population of the V3 INs (Fig.1H–J). These observations confirmed that two subtypes of V3
140 INs found by scRNA-seq are spatially, and probably also functionally, distinct populations in
141 the developing spinal cord.

142

143 *Gene expression profile of V3 IN in zebrafish is distinct from that in amniotes*

144 Next, we analyzed the scRNA-seq data derived from zebrafish whole embryos at 1 and 2
145 day post fertilization (dpf) (Farnsworth et al., 2020) to determine whether V3 INs of zebrafish
146 are equivalent to those of amniotes. We extracted the data with the spinal cord profiles (detailed
147 procedure of the data subsetting is provided in Fig.S1). Similarly to the data analysis of the
148 mouse spinal cord, clustering and dimensionality reduction were applied (Fig.2). In the tSNE

149 plot, the progenitor cells, which mainly consist of 1 dpf cells, were identified by the expression
150 of *sox3* and non-expression of *elavl3* (*HuC*) (Fig.2, Clusters 0, 3, 4, 7, 11, 15, and 17).
151 Expression of the domain specific TFs, such as *pax6b*, *olig2* and *nkx2.2b*, were localized at the
152 specific space in the tSNE plot, which is parallel to the expression domain *in vivo* along the
153 dorsoventral axis of the neural tube (Fig.2, Fig.S2). These data corroborate the evolutionary
154 conservation of the progenitor domain organization in the neural tube (Cheesman and Eisen,
155 2004; Cheesman et al., 2004; Gribble et al., 2007; Guner and Karlstrom, 2007; Lewis et al.,
156 2005; Park et al., 2002; Schäfer et al., 2005). V3 INs can be distinguished by the expression of
157 *sim1a* (magenta circle in Fig.2). These V3 INs were *slc17a6b* positive glutamatergic neurons,
158 like amniotes. However, unlike amniotes, almost all V3 INs expressed *robo3* in zebrafish, and
159 there was no expression of *olig3* and *cntn2*. The expression of *Lhx1* and *Robo3* was mutually
160 exclusive in the amniotes, yet this was not the case in the zebrafish. Furthermore, *neurog3*, one
161 of the V3 IN specific TFs (Carcagno et al., 2014), was not expressed in the V3 INs of zebrafish
162 (Fig.2, compared to Fig.1). These results indicate that V3 INs of zebrafish are not equivalent
163 to those of amniotes so far as the gene expressions are compared.
164
165 *CRM in Robo3 locus is not conserved in teleosts*
166 Focusing on *robo3* in zebrafish, *mnx1* positive MNs (black circle in Fig.2) also expressed
167 *robo3*. This is clearly different from amniotes, in which *Robo3* is never expressed in MNs
168 (Friocourt et al., 2019), implying that the transcriptional regulation of *Robo3* has diverged
169 during vertebrate evolution. To confirm this, we searched for the transcription regulatory
170 elements around *Robo3* locus using the available ChIP-seq and ATAC-seq data of neural cells
171 (Fig.3). We found the putative *cis*-regulatory module (CRM) harboring multiple TF binding
172 sites in an open chromatin state at around 20 kb upstream of *Robo3* transcription start site (TSS)
173 (Fig. 3, CRM in *Robo3* locus is abbreviated as *Robo3-CRM*). To confirm the function of *Robo3-*

174 *CRM*, reporter assay was performed using chick *in ovo* electroporation system. We cloned
175 *Robo3-CRM* from mouse genome into vector containing minimal promoter and *GFP* (resulting
176 construct is named *Robo3-CRM::GFP*). In the chick spinal cord after the electroporation of
177 *Robo3-CRM::GFP*, GFP expression was observed to overlap the endogenous *ROBO3*
178 expression, and GFP positive axons crossed the midline (Fig.3). More specifically, we found
179 that GFP was expressed in LHX1 positive dorsal and intermediate INs, EVX1 positive V0 INs,
180 and NKX2-2 positive V3 INs, but not in ISL1/2 positive dI3 INs or MNs, consistent with the
181 endogenous *ROBO3* expressing cells (Fig.3) (Tulloch et al., 2019). These results demonstrate
182 that *Robo3-CRM* can recapitulate the normal expression pattern of *Robo3* almost completely
183 in the spinal cord.

184 Notably, when sequence conservation was checked using Multiz alignments in UCSC
185 genome browser among vertebrates (Blanchette et al., 2004), *Robo3-CRM* was conserved in
186 tetrapods, but not in teleosts (Fig.3). Weak conservation of *Robo3-CRM* was observed in
187 spotted gar, a basal actinopterygian (Fig.S3), suggesting that common ancestor of bony
188 vertebrates possess *Robo3-CRM*, which has been lost in teleost lineage (Lee et al., 2011). These
189 results suggest that divergent expression patterns of *robo3* in zebrafish are likely due to loss of
190 *Robo3-CRM*. In addition, divergence of *Robo3-CRM* suggests that a part of axon guidance
191 mechanisms in the post-mitotic neurons might have diverged during vertebrate evolution.

192

193 *Non-conservation of GBSs in Gli1 and Ptch1 loci in vertebrates*

194 Next, we examined whether the upstream process before the progenitor fate specification
195 has also diverged among vertebrates. Previous studies have reported that the impacts of loss of
196 Gli function on the neuronal progenitors are different between mice and zebrafish
197 (Chandrasekhar et al., 1999; Karlstrom et al., 2003; Tyurina et al., 2005; Vanderlaan et al.,
198 2005; Wang et al., 2013). This raises the possibility that some Gli binding sites (GBSs), that is,

199 the sites of action of Hh signaling, vary among vertebrates. To test this, *Gli1* and *Ptch1* loci
200 were interrogated, as these genes are direct targets of Hh signaling. We searched for GBS in
201 mouse genome and checked the sequence conservation using Maltiz alignments in the UCSC
202 genome browser. Using Gli1 and Gli3 ChIP-seq data, many GBSs were identified in mouse
203 *Gli1* and *Ptch1* loci near TSS and within intron (Fig.4), confirming previous reports (Dai et al.,
204 1999; Nishi et al., 2015). ATAC-seq data confirmed that these GBSs are in an open chromatin
205 state in neural cells. We found that most of these GBSs are not conserved among vertebrates.
206 In the case of *Gli1*, clustered GBSs are conserved only in mammals, and in the *Ptch1* locus,
207 most GBSs are conserved only in tetrapods, but were lost in teleosts (Fig.4, highlighted region).
208 These findings imply that GBS is highly flexible element. This may partly explain the
209 discrepancy of the *Gli* loss of function phenotypes between mice and zebrafish.
210
211 *Non-conservation of CRMs of progenitor fate specifying TFs in vertebrates*
212 Since the regulatory elements in *Robo3*, *Gli1* and *Ptch1* are not conserved among
213 vertebrates, we expect that non-conservation of the regulatory elements can be found in other
214 genes. Thus, we applied the same analysis to TFs functioning as progenitor fate determinants
215 expressed in the neural tube. Indeed, we found that *Pax6-CRM*, *Gsx1-CRM*, *Dbx2-CRM*, *Irx3-*
216 *CRMs* (2 CRMs, designated *Irx3-CRM1* and *2*), and *Olig2-CRMs* (2 CRMs, designated *Olig2-*
217 *CRM1* and *2*) are conserved only in tetrapods, but were lost in teleosts (Fig.5, highlighted
218 regions). These CRMs are in an open chromatin state in most cases, and are bound by Gli1,
219 Gli3, Sox2, Neurog2, Pax6, Pax7, Olig2, Nkx2-2 and Nkx6-1 in various combinations (Fig.5).
220 These TFs are essential components of GRN, regulating the progenitor fate in the neural tube
221 (Balaskas et al., 2012; Delás and Briscoe, 2020; Exelby et al., 2021; Kutejova et al., 2016).
222 Thus, we consider that non-conservation of these CRMs and conservation of progenitor
223 organization has necessarily entailed the CRM turnover and GRN rewiring during vertebrate

224 evolution. To exclude the possibility that these CRMs has been lost due to having no functions,
225 we carried out the reporter assay by means of the chick *in ovo* electroporation system. This
226 experiment confirmed that *Pax6-CRM*, *Gsx1-CRM*, *Dbx2-CRM*, *Irx3-CRM2*, and *Olig2-CRM2*
227 function as enhancers in the neural tube cells, although more regulatory elements are needed
228 to precisely recapitulate the endogenous expression pattern (Fig.6). Note that this method
229 cannot capture the microRNA-based translational repression, which indeed affects the dorsal
230 boundary of Olig2 (Chen et al., 2011). The only exception was *Irx-CRM1*, which exerted no
231 enhancer function in the chick neural tube (data not shown). Enhancer function of *Olig2-CRM1*
232 was already validated previously (Exelby et al., 2021; Oosterveen et al., 2012; Peterson et al.,
233 2012; Wang et al., 2011). These results indicate that these CRMs are functional in amniotes,
234 but nevertheless were lost in teleosts. This supports the notion that the progenitor fate
235 specification system in the neural tube has undergone CRM turnover and GRN rewiring during
236 vertebrate evolution (Fig.7).
237

238 **Discussion**

239 *Divergent properties of post-mitotic neurons in vertebrates*

240 First, in the current study, we compared the single-cell transcriptomes of mice and
241 zebrafish to elucidate the divergence of the post-mitotic neuronal differentiation. We found
242 that, in amniotes, V3 INs can be divided into two distinct subtypes. One is located medially
243 and expresses *Robo3*, *Olig3*, and *Cntn2*, and the other is located laterally and expresses *Lhx1*
244 (Fig.1). We tried to make these V3 INs correspond with those of zebrafish, but were
245 unsuccessful (Fig.1,2). This indicates that V3 INs of amniotes is not equivalent to those of
246 zebrafish, at least regarding gene expression profile, which supports the hypothesis that the
247 properties of post-mitotic neurons in the spinal cord have diverged among vertebrates. This is
248 in contrast to the case of progenitor cells, in which each progenitor domain of zebrafish readily

249 corresponds with those of amniotes (Fig.S2).

250 The role of V3 INs in mice is to secure the stable locomotor rhythm (Zhang et al., 2008).
251 Several studies have also suggested that V3 INs contribute to left-right synchronous motor
252 output, such as gallop and bound (Danner et al., 2019; Kiehn, 2016; Rabe et al., 2009). These
253 gaits can be expressed by quadrupeds, but not by fish. This suggests that the different locomotor
254 behavior between amniotes and teleosts is associated with the divergence of V3 IN properties.
255 The same may be the case with V2a INs, whose roles have diverged between amniotes and
256 teleosts (Azim et al., 2014; Crone et al., 2008, 2009; Eklöf-Ljunggren et al., 2012; Kiehn,
257 2016). Given that the numbers of muscles and corresponding MNs have significantly increased
258 during tetrapod evolution, especially regarding limb muscles (Diogo and Abdala, 2010),
259 additional layers of neuronal circuits were required to precisely control complex locomotor
260 behavior (Kiehn, 2016). This may be accomplished, at least in part, by tinkering with the
261 already existing neuronal population (Jacob, 1977), eventually leading to the divergence of the
262 post-mitotic neuronal properties among vertebrates. Distinct expression profiles of *Robo3*
263 between amniotes and zebrafish may be one of the strategies for neuronal tinkering (Fig.1–3).
264

265 *Divergent processes leading to the conserved progenitor domains*

266 In the latter part of this study, we investigated the transcriptional regulatory elements
267 located around the progenitor fate specifying genes in order to reveal to what extent the
268 upstream process before the progenitor specification has diverged in vertebrates. In *Gli1* locus,
269 clustered GBSs near the TSS are conserved only in mammals, but not in teleosts (Fig.4). Even
270 in birds and reptiles, these GBSs are conserved only partially. Nevertheless, *Gli1* is expressed
271 in response to Hh signaling commonly in vertebrates (Aglyamova and Agarwala, 2007;
272 Karlstrom et al., 2003; Luo et al., 2006), suggesting the presence of distinct GBSs with
273 equivalent function. Indeed, zebrafish possesses three GBSs in *Gli1* locus, which are conserved

274 only in some teleost species (Wang et al., 2013), indicating that regions where Hh signaling is
275 eventually transduced has shifted during vertebrate evolution. This is supported by a similar
276 situation in *Ptch1* locus (Fig.4) (Wang et al., 2013). Bicoid is a morphogen that plays a crucial
277 role for the patterning of the anterior-posterior axis in *Drosophila* blastoderm, and there are
278 fundamental similarities between Bicoid and Shh (Briscoe and Small, 2015). It is noteworthy
279 that Bicoid binding sites have also undergone rapid turnover in Diptera (McGregor et al., 2001).
280 The flexibility of morphogen response elements might contribute to the integration of the
281 morphogen dependency into the patterning system of the embryo (Dearden and Akam, 1999;
282 Miyamoto and Wada, 2013; Ren et al., 2020; Stauber et al., 1999).

283 In *Pax6*, *Gsx1*, *Dbx2*, *Irx3*, and *Olig2* loci in mouse genome, we identified functional
284 CRMs bound by multiple TFs (Fig.5,6). These CRMs are conserved only in tetrapods, but were
285 lost in teleosts (Fig.5). Given that the progenitor domain organization is conserved among
286 vertebrates, these findings indicate the CRM turnover and GRN rewiring during vertebrate
287 evolution (Fig.7). This is considered to be a case of developmental system drift (DSD) (True
288 and Haag, 2001). Several studies have reported similar situations, in which divergent regulatory
289 sequences in different species result in the conserved gene expressions (Barrière et al., 2012;
290 Fisher et al., 2006; Hare et al., 2008; Ludwig et al., 1998, 2000; Paris et al., 2013; Stolfi et al.,
291 2014; Swanson et al., 2011). In these cases, including the present study, GRN architecture is
292 likely to be maintained as a whole despite the CRM turnover, as demonstrated in mammalian
293 evolution (Stergachis et al., 2014; Vierstra et al., 2014).

294 The process of the neural tube formation is different between amniotes and zebrafish not
295 only genetically, but also morphogenetically. In amniotes, a midline groove is formed by
296 bending of the neural plate, the edges of which are then fused, thus forming the neural tube
297 (Schoenwolf and Smith, 1990). On the other hand, in zebrafish, the solid neural keel with no
298 central canal is formed by convergent movement of the neural plate cells, and then the central

canal opens secondarily (Schmitz et al., 1993). Taken together, the neural tube formation is a case of DSD from both genetic and morphogenetic viewpoints.

Molecular basis of the hourglass model in the spinal cord

Taken together, our results demonstrate that divergence of the developmental process of the spinal cord is in accordance with the developmental hourglass model. Then, what impose the hourglass-like pattern on the evolution of spinal cord development? The progenitor regionalization in the neural tube is a highly robust developmental system, and thus is insensitive against noises and mutations (Balaskas et al., 2012; Delás and Briscoe, 2020; Exelby et al., 2021; Xiong et al., 2013; Zagorski et al., 2017). Simulation studies have also proposed that the developmental system robustness is an emergent property of the complex GRN (Bergman and Siegal, 2003; von Dassow et al., 2000; Siegal and Bergman, 2002), indirectly supporting the robustness of the neuronal progenitor specification system, which is organized by highly complex GRN (Kutejova et al., 2016). From the evolutionary perspective, such a robust (canalized) developmental system can accommodate genetic variations without disturbing development (Rutherford and Lindquist, 1998; Waddington, 1942, 1957). In other words, the progenitor specification system in the neural tube buffers the genetic variations. We speculate that this situation consequently led to the CRM turnover and GRN rewiring, while the progenitor arrangement was maintained. Once cells are released from the progenitor domains as post-mitotic neurons, individual neurons depend on the mechanisms regulating post-mitotic maturation which is distinct from the progenitor specification GRN. As mentioned before, the maturation process is considered to diverge in association with locomotor divergence. Eventually, through vertebrate evolution, developmental divergence of the spinal cord might lead to the hourglass shape. The focus of the current study was the spinal cord. Thus, it is of particular interest to examine whether this scenario is also the case in other

developmental systems or even in whole embryonic level.

More importantly, if partial modification is admitted, neuroectodermal regionalization is conserved among bilaterians beyond vertebrates (Arendt, 2018; Denes et al., 2007; Jung and Dasen, 2015). This suggests that the developmental system robustness of neuroectodermal regionalization had already been acquired in the last common ancestor of bilaterians, and that upstream signals of the neuroectodermal regionalization had been modified after divergence of phyla (e.g., Hh signalling recruitment in deuterostomes) (Miyamoto and Wada, 2013; Ren et al., 2020). This is supported by the notion of the common origin of the central nervous system (CNS) in bilaterians (Arendt, 2018; Arendt et al., 2016; Denes et al., 2007), but is inconsistent with the convergent evolution of CNS (Martín-Durán et al., 2018).

Acknowledgements

We thank Y. Watanabe and T. Shimada for technical supports. This work was supported by JSPS KAKENHI Grant Number 18K14718 and 18K06835. Computations were partially performed on the NIG supercomputer at ROIS National Institute of Genetics. The monoclonal antibodies 74.5A5, 4F2, 3A10, 39.4D5, 99.1-3A2, PAX6, and DSHB-GFP-4C9, developed by T. M. Jessell, J. Dodd, S. Brenner-Morton, A. Kawakami and DSHB were obtained from the Developmental Studies Hybridoma Bank, created by the NICHD of the NIH and maintained at The University of Iowa, Department of Biology, Iowa City, IA 52242.

Author Contributions

Conceptualization, K.M.; Methodology, K.M.; Formal Analysis, K.M.; Investigation, K.M. and C.S.; Writing - Original Draft, K.M.; Writing - Review & Editing, K.M and H.Y.; Funding Acquisition, K.M. and H.Y.

349 **Declaration of Interests**

350 The authors declare no competing interests.

351

352 **Figure Legends**

353 **Figure 1. Two distinct subtypes of V3 INs in amniotes**

354 (A) tSNE plot showing the cells with V3 IN identity derived from mouse embryonic spinal
355 cord. Expression levels of genes indicated are visualized on the tSNE plot. Top right panel
356 shows the result of graph-based clustering with each cluster being colored differently. Cluster
357 numbers (0–11) are labeled. Middle right panel shows embryonic day when cells are corrected.
358 (B–G) Expressions of NKX2-2, *SIM1* and *ROBO3* were examined in the chick spinal cord at
359 the forelimb level at HH25–26. Growing axons were visualized by monoclonal antibody 3A10.
360 Staining of *in situ* hybridization and immunohistochemistry was colored by blue and brown,
361 respectively. C, E and G show the enlarged views of the boxed areas in B, D, and F, respectively.
362 (H–J) Immunohistochemistry using NKX2-2 and LHX1 antibodies. (K)
363 Immunohistochemistry using NKX2-2 and 3A10 antibodies. Ventral-most region of the spinal
364 cord is shown in H–K. Scale bar: 100 μm in F for B, D and F, in K for H–K.

365

366 **Figure 2. Gene expression profile of V3 IN in zebrafish is distinct from that in amniotes**

367 tSNE plot showing the cells with spinal cord identity derived from zebrafish embryos (1
368 and 2 dpf). Top left panel shows the result of graph-based clustering with each cluster being
369 colored differently. Cluster numbers (0–18) are labeled. Top right panel shows embryonic day
370 when cells are corrected. Left-most panel in second row shows progenitors and post-mitotic
371 neurons by distinct color. D and V indicate dorsal and ventral, respectively. Other panels show
372 the expression levels of genes indicated. Magenta and black circles indicate V3 INs and MNs,
373 respectively.

374

375 **Figure 3. CRM in *Robo3* locus is not conserved in teleosts**

376 (A) ChIP-seq and ATAC-seq peak call results are displayed in UCSC genome browser
377 with Multiz Alignments track. *Robo3* locus in mouse genome (mm10) is displayed. Region
378 harboring multiple TF binding sites (*Robo3-CRM*) is highlighted by magenta. Maltiz
379 Alignment track of tatrapods and teleosts are highlighted by different colors. (B–I) *Robo3-*
380 *CRM::GFP* was electroporated into chick neural tube. (B,C) Expression of GFP and *ROBO3*
381 was examined at HH20 (B) and HH25 (C) after electroporation. (D–I) Expression of GFP and
382 TFs indicated was examined at HH25 after electroporation. Scale bar: 100 μm in C for B and
383 C, in I for D–I.

384

385 **Figure 4. Non-conservation of GBSs in *Gli1* and *Ptch1* loci in vertebrates**

386 Gli1/3 ChIP-seq and ATAC-seq peak call results are displayed in UCSC genome browser
387 with Multiz Alignments track. *Gli1* and *Ptch1* loci in mouse genome (mm10) are shown. In
388 *Gli1* locus, magenta region indicates the open chromatin region which is bound by Gli1/3, and
389 is conserved only in mammals. Maltiz Alignment track of mammals and non-mammals are
390 highlighted by different colors. In *Ptch1* locus, magenta regions indicate the open chromatin
391 regions which are bound by Gli1/3, and are conserved only in tetrapods. Maltiz Alignment
392 track of tatrapods and teleosts are highlighted by different colors.

393

394 **Figure 5. Non-conservation of CRMs of progenitor fate specifying TFs in vertebrates**

395 ChIP-seq and ATAC-seq peak call results are displayed in UCSC genome browser with
396 Multiz Alignments track (display mode is dense). Mouse *Pax6*, *Gsx1*, *Dbx2*, *Irx3* and *Olig2*
397 loci are displayed. Regions harboring multiple TF binding sites (CRMs) are highlighted by
398 magenta, and are conserved only in tetrapods. In *Irx3* and *Olig2* loci, two distinct CRMs are

399 numbered 1 and 2 under the track. In *Pax6*, *Dbx2* and *Olig2* loci, previously validated CRMs
400 are indicated by open triangle under the track (Oosterveen et al., 2012; Peterson et al., 2012).
401
402 **Figure 6. Enhancer functions of CRMs of progenitor fate specifying TFs**
403 CRM reporter vectors indicated were electroporated into chick neural tube together with
404 *CAGGS::mCherry* as control vector. (A–J) GFP and mCherry expression were examined at
405 HH19-20 in the forelimb level neural tube. (K–O) The endogenous expression of genes
406 indicated were examined by *in situ* hybridization (L, M, N) or immunohistochemistry (K, O)
407 together with GFP expression. These five CRMs displayed enhancer functions, though GFP
408 expression domains incompletely overlapped with endogenous expression domain. *Pax6-CRM*
409 induced GFP expression almost ubiquitously, yet the expression was not observed in the roof
410 plate (A, F, K). *Gsx1-CRM* induced GFP expression in the dorsal neural tube, but did not induce
411 in the more ventral region than the endogenous expression domain (B, G, L). GFP expression
412 domains induced by *Dbx2-CRM* or *Irx3-CRM2* overlapped with the endogenous expression
413 domain almost completely (C, D, H, I, M, N). *Olig2-CRM2* induced the GFP expression in the
414 intermediate to ventral region, which partially overlapped with, but was more dorsal than, the
415 endogenous expression domain (E, J, O). Scale bar: 100 μm.
416
417 **Figure 7. The hourglass-like pattern of the developmental divergence of the spinal cord**
418 A summary of the present study is shown. In this drawing, development proceeds from
419 bottom to top. Only five progenitor domains are set up, for simplification. Bottom drawing
420 represents the GRNs regulating the progenitor domain establishment. CRMs (indicated by open
421 boxes) located in the progenitor fate specifying genes (*GeneA–D*) has diverged (turnover)
422 between amniotes and teleosts. Accordingly, these GRNs have been rewired, which is
423 considered to be DSD. Nevertheless, these distinct GRNs result in the same progenitor domain

organization due to the developmental system robustness. Top drawing represents the divergence of the differentiation process of post-mitotic neurons. After individual cells leave the progenitor domains as post-mitotic neurons, some neurons undergo distinct maturation process between amniotes and teleosts. Thus, there exist neuronal subpopulations whose function is different between amniotes and teleosts.

Methods

Experimental animals

Fertilized chicken eggs were obtained from Takeuchi farm (Nara, Japan) and incubated at 38°C in a humidified incubator. Embryos were staged according to Hamburger-Hamilton stage series (Hamburger and Hamilton, 1951). All animal experiments were performed in accordance with the Rules of Fukushima Medical University Animal Experiments, with approval of the Animal Experiments Committee of Fukushima Medical University (approval number 2020103).

scRNA-seq data analysis

Mouse spinal cord scRNA-seq data (Delile et al., 2019) was obtained from ArrayExpress (accession number E-MTAB-7320). UMI count matrix was generated using Cell Ranger version 3.1.0 (10x Genomics). In this step, normalization was skipped in order to maximize sensitivity (cellranger aggr was executed with --normalize=none). The output matrix was fed into Seurat (R package) version 3.1.5 (Butler et al., 2018). Zebrafish whole embryo scRNA-seq data (Farnsworth et al., 2020) was obtained as Seurat object (.rds file) from Dr. Miller's website (https://www.adammillerlab.com/resources-1). Detailed procedures of normalization, data subsetting, graph-based clustering, and dimensionality reduction using Seurat are provided in https://github.com/kmukaigasa/Spinalcord_MouseZebrafish.

449

450 *ChIP-seq data analysis*

451 ChIP-seq data were obtained from NCBI sequence read archive (SRA). The accession
452 numbers are as follows: GSE66961 for Pax6 (Sun et al., 2015); GSE42132 for Sox2 and Gli1
453 (Peterson et al., 2012); GSE61673 for Gli3, Nkx2-2, Nkx6-1, and Olig2 (Nishi et al., 2015);
454 GSE114172 for Neurog2 (Aydin et al., 2019); and GSE87180 for Pax7 (Mayran et al., 2018).
455 The cell types used were embryonic forebrain (Pax6), AtT-20 cell (Pax7), and neural cells
456 differentiated from mouse ES cells (Sox2, Gli1/3, Nkx2-2, Nkx6-1, Olig2, Neurog2).
457 Sequencing adaptors and low quality bases were trimmed by Trimmomatic (version 0.39).
458 FastQC (version 0.11.9) was used for sequence quality check. Read mapping to mouse
459 reference genome (mm10) was performed by Bowtie2 (version 2.3.5) with default setting.
460 Reads with low mapping quality (MAPQ < 10) were removed by samtools (version 1.9). Peak
461 call was performed by MACS2 (version 2.2.6). Output bedGraph file was converted to BigWig
462 format by bdg2bw (https://gist.github.com/jl32587/34370c995460f9d5ad65). BigWig track
463 was visualized in UCSC genome browser.

464

465 *ATAC-seq data analysis*

466 ATAC-seq data (Metzis et al., 2018) were obtained from ArrayExpress (E-MTAB-6337).
467 From the dataset, data of the neural progenitor cells with spinal cord identity were used. Read
468 quality control was done as ChIP-seq. Read mapping was performed by Bowtie2 with the
469 following parameters; -X 2000 --sensitive-local. PCR duplicates were marked using Picard
470 (version 2.9.2). Reads with low mapping quality (MAPQ < 30) were removed by samtools.
471 Peak call was performed by MACS2 with following parameters; -f BAMPE -g mm -q 0.05 --
472 nomodel --keep-dup auto -B.

473

474 *Comparison of genomic sequence by VISTA*

475 For interspecies comparison of genomic sequence, partial genomic sequences were
476 obtained from UCSC genome browser (https://genome.ucsc.edu) and Ensembl
477 (https://www.ensembl.org/index.html), and VISTA (Frazer et al., 2004) are used to align and
478 visualize the results.

479

480 *Vector construction*

481 For RNA probe preparation, partial fragments of *ROBO3*, *IRX3*, *DBX2*, and *GSX1* were
482 amplified by PCR from chick embryonic spinal cord cDNA. The primer sequences used are
483 provided in Table S2. The fragments were inserted into pCR-XL-TOPO (Thermo Fisher) or
484 *pBluescriptKS*. For reporter assay of CRMs, genomic DNA fragments were amplified by PCR
485 from a solution which was prepared by digesting the tail tip of a C57BL/6J mouse. The
486 amplified fragments were inserted into *pSF-pA-MinProm-eGFP* vector (Oxford genetics).
487 Positions of CRMs within the mouse reference genome are provided in Table S3. For
488 construction of *pCAGGS-mCherry*, *mCherry* gene cassette of *pmCherry-C1* (Clontech) was
489 inserted into *pCAGGS* (Niwa et al., 1991).

490

491 *in ovo electroporation*

492 A small window was opened on the top of the fertilized chicken egg shell. The electrodes
493 were placed on both sides of the neural tube of a HH12-13 chick embryo. Plasmid DNA was
494 injected into the neural tube. During injection, electric pulses (25 V, 50 ms, five times, 950 ms
495 interval) were applied using CUY21EDIT (BEX, Tokyo, Japan). Plasmids were prepared at 1
496 μg/μl for *pSF-Robo3-CRM::GFP*, 20–50 ng/μl for *pSF-Pax6-CRM::GFP*, *pSF-Gsx1-*
497 *CRM::GFP*, *pSF-Dbx2-CRM::GFP*, *pSF-Irx3-CRM::GFP*, *pSF-Olig2-CRM::GFP*, 0.5 ng/μl
498 for *pCAGGS-mCherry*.

499

500 *Immunohistochemistry*

501 Embryos were fixed in 0.1 M phosphate buffer / 4% paraformaldehyde (PFA) at room
502 temperature for 45–60 min or 4°C overnight. The fixed embryos were then cryoprotected in
503 20% sucrose at 4°C overnight, embedded in OCT compound, and cryosectioned. In cases of
504 overnight fixed samples, sections were boiled for 20 min in sodium citrate buffer (10 mM
505 sodium citrate, 0.05% Tween 20, pH 6.0) and cooled down to room temperature. After washing
506 with phosphate-buffered saline (PBS) containing 0.1% Triton X-100 (PBST), the sections were
507 incubated with primary antibodies at 4°C overnight, washed with PBST three times for 5 min,
508 and incubated with secondary antibodies for 1–2 h at room temperature. After washing with
509 PBST three times for 5 min, slides were coverslipped in VECTASHIELD (Vector laboratories).
510 The antibodies used are described in Table S4. In the cases of anti-Pax6 and anti-Lhx1, Can
511 Get Signal (TOYOBO, NKB-401) was used for the diluent instead of PBST. Images were
512 captured using an Olympus BX51 fluorescent microscope equipped with an Olympus DP71
513 digital camera, or an Olympus FluoView FV1000 confocal microscope.

514

515 *in situ hybridization*

516 For double staining of immunohistochemistry and *in situ* hybridization,
517 immunohistochemistry was performed as described above with primary and secondary
518 antibody incubation for 1 h at room temperature, and signal was developed by VECTASTAIN
519 Elite ABC kit (Vector laboratories). Following that, the process of *in situ* hybridization, as
520 described below, was started. Plasmid for RNA probe template was linearized, and DIG-labeled
521 RNA probes were generated using DIG RNA labeling mix (Sigma-Aldrich, 11277073910) and
522 T3 RNA polymerase (Promega, P2083).

523 Tissue slides were washed with PBS for 5 min, treated with protainaseK (2μg/ml) for 10

524 min, washed with PBS for 5 min, fixed in 4% PFA for 10 min, and washed three times with
525 PBS for 5 min. The slides were then incubated in an acetylation solution (100 mM
526 triethanolamine, pH 8.0) twice for 2–3 min, transferred in new acetylation solution and
527 acetylated for 15 min by adding dropwise acetic anhydride (0.3% final concentration), and
528 washed with PBS three times for 5 min. The slides were prehybridized with hybridization
529 buffer (50% formamide, 5X SSC, 5X Denhardt's, 500 μg/ml herring sperm DNA, 250 μg/ml
530 yeast RNA) for 2–3 h at room temperature, and hybridized with hybridization buffer containing
531 DIG-labelled RNA probe. The slides were coverslipped and incubated in a humidified chamber
532 at 70°C overnight. The following day, the slides were transferred in 5X SSC at 70°C for 5 min,
533 washed twice in 0.2X SSC for 30 min at 70°C, and washed in 0.2X SSC for 30 min at room
534 temperature. Slides were washed with buffer B1 (100mM Tris-HCl pH 7.5, 150 mM NaCl,
535 0.1% Tween 20) three times for 30 min, incubated with buffer B1 containing 10% heat-
536 inactivated normal goat serum for 2–3 h at room temperature, and then incubated with buffer
537 B1 containing alkaline phosphatase conjugated anti-DIG antibody (Roche 11093274910,
538 1:5000) and 1% heat-inactivated normal goat serum at 4°C overnight. The following day, slides
539 were washed five times with buffer B1 for 30 min, and incubated in buffer B3 (100 mM Tris-
540 HCl pH 9.5, 100 mM NaCl, 50 mM MgCl2, 0.1% Tween20) three times for 5 min. The slides
541 were incubated with BM purple (Roche, 11442074001) until the signal was visualized (3 h to
542 overnight). After that, the slides were washed three times with buffer B1 for 30 min, then
543 washed three times with PBS for 5 min, and coverslipped in Fluoromount (Diagnostic
544 Biosystems, K024).
545

546 **References**

547 Aglyamova, G. V., and Agarwala, S. (2007). Gene expression analysis of the Hedgehog
548 signaling cascade in the chick midbrain and spinal cord. Dev. Dyn. *236*, 1363–1373.

549 Andrews, M.G., Kong, J., Novitch, B.G., and Butler, S.J. (2019). New perspectives on the
550 mechanisms establishing the dorsal-ventral axis of the spinal cord. Curr. Top. Dev. Biol. *132*,
551 417–450.
552 Arendt, D. (2018). Animal Evolution: Convergent Nerve Cords? Curr. Biol. *28*, R225–R227.
553 Arendt, D., Tosches, M.A., and Marlow, H. (2016). From nerve net to nerve ring, nerve cord
554 and brain-evolution of the nervous system. Nat. Rev. Neurosci. *17*, 61–72.
555 Aydin, B., Kakumanu, A., Rossillo, M., Moreno-Estellés, M., Garipler, G., Ringstad, N.,
556 Flames, N., Mahony, S., and Mazzoni, E.O. (2019). Proneural factors Ascl1 and Neurog2
557 contribute to neuronal subtype identities by establishing distinct chromatin landscapes. Nat.
558 Neurosci. *22*, 897–908.
559 Azim, E., Jiang, J., Alstermark, B., and Jessell, T.M. (2014). Skilled reaching relies on a V2a
560 propriospinal internal copy circuit. Nature *508*, 357–363.
561 Balaskas, N., Ribeiro, A., Panovska, J., Dessaud, E., Sasai, N., Page, K.M., Briscoe, J., and
562 Ribes, V. (2012). Gene regulatory logic for reading the Sonic Hedgehog signaling gradient in
563 the vertebrate neural tube. Cell *148*, 273–284.
564 Barrière, A., Gordon, K.L., and Ruvinsky, I. (2012). Coevolution within and between
565 Regulatory Loci Can Preserve Promoter Function Despite Evolutionary Rate Acceleration.
566 PLoS Genet. *8*, e1002961.
567 Bergman, A., and Siegal, M.L. (2003). Evolutionary capacitance as a general feature of
568 complex gene networks. Nature *424*, 549–552.
569 Blanchette, M., Kent, W.J., Riemer, C., Elnitski, L., Smit, A.F.A., Roskin, K.M., Baertsch,
570 R., Rosenbloom, K., Clawson, H., Green, E.D., et al. (2004). Aligning multiple genomic
571 sequences with the threaded blockset aligner. Genome Res. *14*, 708–715.
572 Briscoe, J., and Small, S. (2015). Morphogen rules: design principles of gradient-mediated
573 embryo patterning. Development *142*, 3996–4009.

574 Briscoe, J., and Thérond, P.P. (2013). The mechanisms of Hedgehog signalling and its roles
575 in development and disease. Nat. Rev. Mol. Cell Biol. *14*, 416–429.
576 Briscoe, J., Sussel, L., Serup, P., Hartigan-O'Connor, D., Jessell, T.M., Rubenstein, J.L.R.,
577 and Ericson, J. (1999). Homeobox gene Nkx2.2 and specification of neuronal identity by
578 graded Sonic hedgehog signalling. Nature *398*, 622–627.
579 Briscoe, J., Pierani, A., Jessell, T., and Ericson, J. (2000). A homeodomain protein code
580 specifies progenitor cell identity and neuronal fate in the ventral neural tube. Cell *101*, 435–
581 445.
582 Butler, A., Hoffman, P., Smibert, P., Papalexi, E., and Satija, R. (2018). Integrating single-
583 cell transcriptomic data across different conditions, technologies, and species. Nat.
584 Biotechnol. *36*, 411–420.
585 Carcagno, A.L., Di Bella, D.J., Goulding, M., Guillemot, F., and Lanuza, G.M. (2014).
586 Neurogenin3 Restricts Serotonergic Neuron Differentiation to the Hindbrain. J. Neurosci. *34*,
587 15223–15233.
588 Challa, A.K., McWhorter, M.L., Wang, C., Seeger, M.A., and Beattie, C.E. (2005). Robo3
589 isoforms have distinct roles during zebrafish development. Mech. Dev. *122*, 1073–1086.
590 Chandrasekhar, A., Schauerte, H.E., Haffter, P., and Kuwada, J.Y. (1999). The zebrafish
591 detour gene is essential for cranial but not spinal motor neuron induction. Development *126*,
592 2727–2737.
593 Cheesman, S.E., and Eisen, J.S. (2004). Gsh1 Demarcates Hypothalamus and Intermediate
594 Spinal Cord in Zebrafish. Gene Expr. Patterns *5*, 107–112.
595 Cheesman, S.E., Layden, M.J., Von Ohlen, T., Doe, C.Q., and Eisen, J.S. (2004). Zebrafish
596 and fly Nkx6 proteins have similar CNS expression patterns and regulate motoneuron
597 formation. Development *131*, 5221–5232.
598 Chen, J.A., Huang, Y.P., Mazzoni, E.O., Tan, G.C., Zavadil, J., and Wichterle, H. (2011).

599 Mir-17-3p Controls Spinal Neural Progenitor Patterning by Regulating Olig2/Irx3 Cross-
600 Repressive Loop. Neuron *69*, 721–735.
601 Crone, S.A., Quinlan, K.A., Zagoraiou, L., Droho, S., Restrepo, C.E., Lundfald, L., Endo, T.,
602 Setlak, J., Jessell, T.M., Kiehn, O., et al. (2008). Genetic Ablation of V2a Ipsilateral
603 Interneurons Disrupts Left-Right Locomotor Coordination in Mammalian Spinal Cord.
604 Neuron *60*, 70–83.
605 Crone, S.A., Zhong, G., Harris-Warrick, R., and Sharma, K. (2009). In mice lacking V2a
606 interneurons, gait depends on speed of locomotion. J. Neurosci. *29*, 7098–7109.
607 Currie, P.D., and Ingham, P.W. (1996). Induction of a specific muscle cell type by a
608 hedgehog-like protein in zebrafish. Nature *382*, 452–455.
609 Dai, P., Akimaru, H., Tanaka, Y., Maekawa, T., Nakafuku, M., and Ishii, S. (1999). Sonic
610 Hedgehog-induced Activation of the Gli1 Promoter Is Mediated by GLI3. J. Biol. Chem. *274*,
611 8143–8152.
612 Danner, S.M., Zhang, H., Shevtsova, N.A., Borowska-Fielding, J., Deska-Gauthier, D.,
613 Rybak, I.A., and Zhang, Y. (2019). Spinal V3 Interneurons and Left–Right Coordination in
614 Mammalian Locomotion. Front. Cell. Neurosci. *13*, 516.
615 von Dassow, G., Meir, E., Munro, E.M., and Odell, G.M. (2000). The segment polarity
616 network is a robust developmental module. Nature *406*, 188–192.
617 Dearden, P., and Akam, M. (1999). Developmental evolution: Axial patterning in insects.
618 Curr. Biol. *9*, R591-R594.
619 Delás, M.J., and Briscoe, J. (2020). Repressive interactions in gene regulatory networks:
620 When you have no other choice. Curr. Top. Dev. Biol. *139*, 239–266.
621 Del Barrio, M.G., Taveira-Marques, R., Muroyama, Y., Yuk, D.-I., Li, S., Wines-Samuelson,
622 M., Shen, J., Smith, H.K., Xiang, M., Rowitch, D., et al. (2007). A regulatory network
623 involving Foxn4, Mash1 and delta-like 4/Notch1 generates V2a and V2b spinal interneurons

624 from a common progenitor pool. Development *134*, 3427–3436.
625 Delile, J., Rayon, T., Melchionda, M., Edwards, A., Briscoe, J., and Sagner, A. (2019). Single
626 cell transcriptomics reveals spatial and temporal dynamics of gene expression in the
627 developing mouse spinal cord. Development *146*, dev173807.
628 Denes, A.S., Jékely, G., Steinmetz, P.R.H., Raible, F., Snyman, H., Prud'homme, B., Ferrier,
629 D.E.K., Balavoine, G., and Arendt, D. (2007). Molecular Architecture of Annelid Nerve Cord
630 Supports Common Origin of Nervous System Centralization in Bilateria. Cell *129*, 277–288.
631 Ding, Q., Motoyama, J., Gasca, S., Mo, R., Sasaki, H., Rossant, J., and Hui, C.C. (1998).
632 Diminished Sonic hedgehog signaling and lack of floor plate differentiation in Gli2 mutant
633 mice. Development *125*, 2533–2543.
634 Ding, Q., Joshi, P.S., Xie, Z.-H., Xiang, M., and Gan, L. (2012). BARHL2 transcription
635 factor regulates the ipsilateral/contralateral subtype divergence in postmitotic dI1 neurons of
636 the developing spinal cord. Proc. Natl. Acad. Sci. U. S. A. *109*, 1566–1571.
637 Diogo, R., and Abdala, V. (2010). Muscles of vertebrates : comparative anatomy, evolution,
638 homologies and development (CRC Press).
639 Duboule, D. (1994). Temporal colinearity and the phylotypic progression: a basis for the
640 stability of a vertebrate Bauplan and the evolution of morphologies through heterochrony.
641 Development *1994*, 135–142.
642 Echelard, Y., Epstein, D.J., St-Jacques, B., Shen, L., Mohler, J., McMahon, J.A., and
643 McMahon, A.P. (1993). Sonic hedgehog, a member of a family of putative signaling
644 molecules, is implicated in the regulation of CNS polarity. Cell *75*, 1417–1430.
645 Ekker, S.C., Ungar, A.R., Greenstein, P., von Kessler, D.P., Porter, J.A., Moon, R.T., and
646 Beachy, P.A. (1995). Patterning activities of vertebrate hedgehog proteins in the developing
647 eye and brain. Curr. Biol. *5*, 944–955.
648 Eklöf-Ljunggren, E., Haupt, S., Ausborn, J., Dehnisch, I., Uhlén, P., Higashijima, S., and El

649 Manira, A. (2012). Origin of excitation underlying locomotion in the spinal circuit of
650 zebrafish. Proc. Natl. Acad. Sci. U. S. A. *109*, 5511–5516.
651 Exelby, K., Herrera-Delgado, E., Garcia Perez, L., Perez-Carrasco, R., Sagner, A., Metzis,
652 V., Sollich, P., and Briscoe, J. (2021). Precision of Tissue Patterning is Controlled by
653 Dynamical Properties of Gene Regulatory Networks. Development *148,* dev197566.
654 Farnsworth, D.R., Saunders, L.M., and Miller, A.C. (2020). A single-cell transcriptome atlas
655 for zebrafish development. Dev. Biol. *459*, 100–108.
656 Fisher, S., Grice, E.A., Vinton, R.M., Bessling, S.L., and McCallion, A.S. (2006).
657 Conservation of RET regulatory function from human to zebrafish without sequence
658 similarity. Science *312*, 276–279.
659 Frazer, K.A., Pachter, L., Poliakov, A., Rubin, E.M., and Dubchak, I. (2004). VISTA:
660 computational tools for comparative genomics. Nucleic Acids Res. *32*, W273–W279.
661 Friocourt, F., and Chédotal, A. (2017). The Robo3 receptor, a key player in the development,
662 evolution, and function of commissural systems. Dev. Neurobiol. *77*, 876–890.
663 Friocourt, F., Kozulin, P., Belle, M., Suárez, R., Di-Poï, N., Richards, L.J., Giacobini, P., and
664 Chédotal, A. (2019). Shared and differential features of Robo3 expression pattern in
665 amniotes. J. Comp. Neurol. *527*, 2009–2029.
666 Gribble, S.L., Nikolaus, O.B., and Dorsky, R.I. (2007). Regulation and function of Dbx genes
667 in the zebrafish spinal cord. Dev. Dyn. *236*, 3472–3483.
668 Guner, B., and Karlstrom, R.O. (2007). Cloning of zebrafish nkx6.2 and a comprehensive
669 analysis of the conserved transcriptional response to Hedgehog/Gli signaling in the zebrafish
670 neural tube. Gene Expr. Patterns *7*, 596–605.
671 Hamburger, V., and Hamilton, H.L. (1951). A series of normal stages in the development of
672 the chick embryo. J. Morphol. *88*, 49–92.
673 Hare, E.E., Peterson, B.K., Iyer, V.N., Meier, R., and Eisen, M.B. (2008). Sepsid even-

674 skipped enhancers are functionally conserved in Drosophila despite lack of sequence
675 conservation. PLoS Genet. *4,* e1000106.
676 Hu, H., Uesaka, M., Guo, S., Shimai, K., Lu, T.-M., Li, F., Fujimoto, S., Ishikawa, M., Liu,
677 S., Sasagawa, Y., et al. (2017). Constrained vertebrate evolution by pleiotropic genes. Nat.
678 Ecol. Evol. *1*, 1722–1730.
679 Irie, N., and Kuratani, S. (2014). The developmental hourglass model: a predictor of the basic
680 body plan? Development *141*, 4649–4655.
681 Jacob, F. (1977). Evolution and tinkering. Science *196*, 1161–1166.
682 Jung, H., and Dasen, J.S. (2015). Evolution of Patterning Systems and Circuit Elements for
683 Locomotion. Dev. Cell *32*, 408–422.
684 Karlstrom, R.O., Trowe, T., Klostermann, S., Baier, H., Brand, M., Crawford, A.D.,
685 Grunewald, B., Haffter, P., Hoffmann, H., Meyer, S.U., et al. (1996). Zebrafish mutations
686 affecting retinotectal axon pathfinding. Development *123*, 427–438.
687 Karlstrom, R.O., Tyurina, O. V., Kawakami, A., Nishioka, N., Talbot, W.S., Sasaki, H., and
688 Schier, A.F. (2003). Genetic analysis of zebrafish gli1 and gli2 reveals divergent
689 requirements for gli genes in vertebrate development. Development *130*, 1549–1564.
690 Ke, Z., Kondrichin, I., Gong, Z., and Korzh, V. (2008). Combined activity of the two Gli2
691 genes of zebrafish play a major role in Hedgehog signaling during zebrafish
692 neurodevelopment. Mol. Cell. Neurosci. *37*, 388–401.
693 Kiehn, O. (2016). Decoding the organization of spinal circuits that control locomotion. Nat.
694 Rev. Neurosci. *17*, 224–238.
695 Krauss, S., Concordet, J.P., and Ingham, P.W. (1993). A functionally conserved homolog of
696 the Drosophila segment polarity gene hh is expressed in tissues with polarizing activity in
697 zebrafish embryos. Cell *75*, 1431–1444.
698 Kutejova, E., Sasai, N., Shah, A., Gouti, M., and Briscoe, J. (2016). Neural Progenitors

699 Adopt Specific Identities by Directly Repressing All Alternative Progenitor Transcriptional
700 Programs. Dev. Cell *36*, 639–653.
701 Lai, H.C., Seal, R.P., and Johnson, J.E. (2016). Making sense out of spinal cord
702 somatosensory development. Development *143*, 3434–3448.
703 Lee, A.P., Kerk, S.Y., Tan, Y.Y., Brenner, S., and Venkatesh, B. (2011). Ancient Vertebrate
704 Conserved Noncoding Elements Have Been Evolving Rapidly in Teleost Fishes. Mol. Biol.
705 Evol. *28*, 1205–1215.
706 Lewis, K.E., Bates, J., and Eisen, J.S. (2005). Regulation of iro3 expression in the zebrafish
707 spinal cord. Dev. Dyn. *232*, 140–148.
708 Li, S., Misra, K., Matise, M.P., and Xiang, M. (2005). Foxn4 acts synergistically with Mash1
709 to specify subtype identity of V2 interneurons in the spinal cord. Proc. Natl. Acad. Sci. U. S.
710 A. *102*, 10688–10693.
711 Lu, D.C., Niu, T., and Alaynick, W.A. (2015). Molecular and cellular development of spinal
712 cord locomotor circuitry. Front. Mol. Neurosci. *8*, 25.
713 Ludwig, M.Z., Patel, N.H., and Kreitman, M. (1998). Functional analysis of eve stripe 2
714 enhancer evolution in Drosophila, rules governing conservation and change. Development
715 *125*, 949–958.
716 Ludwig, M.Z., Bergman, C., Patel, N.H., and Kreitman, M. (2000). Evidence for stabilizing
717 selection in a eukaryotic enhancer element. Nature *403*, 564–567.
718 Luo, J., Ju, M.J., and Redies, C. (2006). Regionalized cadherin-7 expression by radial glia is
719 regulated by Shh and Pax7 during chicken spinal cord development. Neuroscience *142*,
720 1133–1143.
721 Marillat, V., Sabatier, C., Failli, V., Matsunaga, E., Sotelo, C., Tessier-Lavigne, M., and
722 Chédotal, A. (2004). The slit receptor Rig-1/Robo3 controls midline crossing by hindbrain
723 precerebellar neurons and axons. Neuron *43*, 69–79.

724 Martín-Durán, J.M., Pang, K., Børve, A., Lê, H.S., Furu, A., Cannon, J.T., Jondelius, U., and
725 Hejnol, A. (2018). Convergent evolution of bilaterian nerve cords. Nature *553*, 45–50.
726 Matise, M.P., Epstein, D.J., Park, H.L., Platt, K.A., and Joyner, A.L. (1998). Gli2 is required
727 for induction of floor plate and adjacent cells, but not most ventral neurons in the mouse
728 central nervous system. Development *125*, 2759–2770.
729 Mayran, A., Khetchoumian, K., Hariri, F., Pastinen, T., Gauthier, Y., Balsalobre, A., and
730 Drouin, J. (2018). Pioneer factor Pax7 deploys a stable enhancer repertoire for specification
731 of cell fate. Nat. Genet. *50*, 259–269.
732 McGregor, A.P., Shaw, P.J., Hancock, J.M., Bopp, D., Hediger, M., Wratten, N.S., and
733 Dover, G.A. (2001). Rapid restructuring of bicoid-dependent hunchback promoters within
734 and between Dipteran species: implications for molecular coevolution. Evol. Dev. *3*, 397–
735 407.
736 Metzis, V., Steinhauser, S., Pakanavicius, E., Gouti, M., Stamataki, D., Ivanovitch, K.,
737 Watson, T., Rayon, T., Mousavy Gharavy, S.N., Lovell-Badge, R., et al. (2018). Nervous
738 System Regionalization Entails Axial Allocation before Neural Differentiation. Cell *175*,
739 1105-1118.e17.
740 Miyamoto, N., and Wada, H. (2013). Hemichordate neurulation and the origin of the neural
741 tube. Nat. Commun. *4*, 2713.
742 Nishi, Y., Zhang, X., Jeong, J., Peterson, K.A., Vedenko, A., Bulyk, M.L., Hide, W.A., and
743 McMahon, A.P. (2015). A direct fate exclusion mechanism by Sonic hedgehog-regulated
744 transcriptional repressors. Development *142*, 3286–3293.
745 Niwa, H., Yamamura, K., and Miyazaki, J. (1991). Efficient selection for high-expression
746 transfectants with a novel eukaryotic vector. Gene *108*, 193–199.
747 Oosterveen, T., Kurdija, S., Alekseenko, Z., Uhde, C.W., Bergsland, M., Sandberg, M.,
748 Andersson, E., Dias, J.M., Muhr, J., and Ericson, J. (2012). Mechanistic Differences in the

749 Transcriptional Interpretation of Local and Long-Range Shh Morphogen Signaling. Dev. Cell
750 *23*, 1006–1019.
751 Panayi, H., Panayiotou, E., Orford, M., Genethliou, N., Mean, R., Lapathitis, G., Li, S.,
752 Xiang, M., Kessaris, N., Richardson, W.D., et al. (2010). Sox1 is required for the
753 specification of a novel p2-derived interneuron subtype in the mouse ventral spinal cord. J.
754 Neurosci. *30*, 12274–12280.
755 Paris, M., Kaplan, T., Li, X.Y., Villalta, J.E., Lott, S.E., and Eisen, M.B. (2013). Extensive
756 Divergence of Transcription Factor Binding in Drosophila Embryos with Highly Conserved
757 Gene Expression. PLoS Genet. *9*, e1003748.
758 Park, H.C., Mehta, A., Richardson, J.S., and Appel, B. (2002). Olig2 Is Required for
759 Zebrafish Primary Motor Neuron and Oligodendrocyte Development. Dev. Biol. *248*, 356–
760 368.
761 Park, H.L., Bai, C., Platt, K.A., Matise, M.P., Beeghly, A., Hui, C.C., Nakashima, M., and
762 Joyner, A.L. (2000). Mouse Gli1 mutants are viable but have defects in SHH signaling in
763 combination with a Gli2 mutation. Development *127*, 1593–1605.
764 Peng, C.Y., Yajima, H., Burns, C.E., Zon, L.I., Sisodia, S.S., Pfaff, S.L., and Sharma, K.
765 (2007). Notch and MAML Signaling Drives Scl-Dependent Interneuron Diversity in the
766 Spinal Cord. Neuron *53*, 813–827.
767 Persson, M., Stamataki, D., te Welscher, P., Andersson, E., Böse, J., Rüther, U., Ericson, J.,
768 and Briscoe, J. (2002). Dorsal-ventral patterning of the spinal cord requires Gli3
769 transcriptional repressor activity. Genes Dev. *16*, 2865–2878.
770 Peterson, K.A., Nishi, Y., Ma, W., Vedenko, A., Shokri, L., Zhang, X., McFarlane, M.,
771 Baizabal, J.-M., Junker, J.P., van Oudenaarden, A., et al. (2012). Neural-specific Sox2 input
772 and differential Gli-binding affinity provide context and positional information in Shh-
773 directed neural patterning. Genes Dev. *26*, 2802–2816.

774 Prince, V.E., Moens, C.B., Kimmel, C.B., and Ho, R.K. (1998a). Zebrafish hox genes:
775 expression in the hindbrain region of wild-type and mutants of the segmentation gene,
776 valentino. Development *125*, 393–406.
777 Prince, V.E., Joly, L., Ekker, M., and Ho, R.K. (1998b). Zebrafish hox genes: genomic
778 organization and modified colinear expression patterns in the trunk. Development *125*, 407–
779 420.
780 Rabe, N., Gezelius, H., Vallstedt, A., Memic, F., and Kullander, K. (2009). Netrin-1-
781 dependent spinal interneuron subtypes are required for the formation of left-right alternating
782 locomotor circuitry. J. Neurosci. *29*, 15642–15649.
783 Ren, Q., Zhong, Y., Huang, X., Leung, B., Xing, C., Wang, H., Hu, G., Wang, Y., Shimeld,
784 S.M., and Li, G. (2020). Step-wise evolution of neural patterning by Hedgehog signalling in
785 chordates. Nat. Ecol. Evol. *4*, 1247–1255.
786 Riddle, R.D., Johnson, R.L., Laufer, E., and Tabin, C. (1993). Sonic hedgehog mediates the
787 polarizing activity of the ZPA. Cell *75*, 1401–1416.
788 Roelink, H., Augsburger, A., Heemskerk, J., Korzh, V., Norlin, S., Ruiz i Altaba, A., Tanabe,
789 Y., Placzek, M., Edlund, T., Jessell, T.M., et al. (1994). Floor plate and motor neuron
790 induction by vhh-1, a vertebrate homolog of hedgehog expressed by the notochord. Cell *76*,
791 761–775.
792 Rutherford, S.L., and Lindquist, S. (1998). Hsp90 as a capacitor for morphological evolution.
793 Nature *396*, 336–342.
794 Sabatier, C., Plump, A.S., Le Ma, Brose, K., Tamada, A., Murakami, F., Lee, E.Y.-H.P., and
795 Tessier-Lavigne, M. (2004). The divergent Robo family protein rig-1/Robo3 is a negative
796 regulator of slit responsiveness required for midline crossing by commissural axons. Cell
797 *117*, 157–169.
798 Sagner, A., and Briscoe, J. (2019). Establishing neuronal diversity in the spinal cord: a time

799 and a place. Development *146*, dev182154.

800 Schäfer, M., Kinzel, D., Neuner, C., Schartl, M., Volff, J.N., and Winkler, C. (2005).
801 Hedgehog and retinoid signalling confines nkx2.2b expression to the lateral floor plate of the
802 zebrafish trunk. Mech. Dev. *122*, 43–56.

803 Schmitz, B., Papan, C., and Campos-Ortega, J.A. (1993). Neurulation in the anterior trunk
804 region of the zebrafish Brachydanio rerio. Roux's Arch. Dev. Biol. *202*, 250–259.

805 Schoenwolf, G.C., and Smith, J.L. (1990). Mechanisms of neurulation: Traditional viewpoint
806 and recent advances. Development *109*, 243–270.

807 Siegal, M.L., and Bergman, A. (2002). Waddington's canalization revisited: developmental
808 stability and evolution. Proc. Natl. Acad. Sci. U. S. A. *99*, 10528–10532.

809 Stauber, M., Jäckle, H., and Schmidt-Ott, U. (1999). The anterior determinant bicoid of
810 Drosophila is a derived Hox class 3 gene. Proc. Natl. Acad. Sci. U. S. A. *96*, 3786–3789.

811 Stergachis, A.B., Neph, S., Sandstrom, R., Haugen, E., Reynolds, A.P., Zhang, M., Byron,
812 R., Canfield, T., Stelhing-Sun, S., Lee, K., et al. (2014). Conservation of trans-acting
813 circuitry during mammalian regulatory evolution. Nature *515*, 365–370.

814 Stolfi, A., Lowe, E.K., Racioppi, C., Ristoratore, F., Brown, C.T., Swalla, B.J., and
815 Christiaen, L. (2014). Divergent mechanisms regulate conserved cardiopharyngeal
816 development and gene expression in distantly related ascidians. Elife *3*, e03728.

817 Sun, J., Rockowitz, S., Xie, Q., Ashery-Padan, R., Zheng, D., and Cvekl, A. (2015).
818 Identification of in vivo DNA-binding mechanisms of Pax6 and reconstruction of Pax6-
819 dependent gene regulatory networks during forebrain and lens development. Nucleic Acids
820 Res. *43*, 6827–6846.

821 Swanson, C.I., Schwimmer, D.B., and Barolo, S. (2011). Rapid evolutionary rewiring of a
822 structurally constrained eye enhancer. Curr. Biol. *21*, 1186–1196.

823 True, J.R., and Haag, E.S. (2001). Developmental system drift and flexibility in evolutionary

824 trajectories. Evol. Dev. *3*, 109–119.

825 Tulloch, A.J., Teo, S., Carvajal, B. V., Tessier-Lavigne, M., and Jaworski, A. (2019). Diverse
826 spinal commissural neuron populations revealed by fate mapping and molecular profiling
827 using a novel Robo3Cre mouse. J. Comp. Neurol. *527*, 2948–2972.

828 Tyurina, O. V., Guner, B., Popova, E., Feng, J., Schier, A.F., Kohtz, J.D., and Karlstrom,
829 R.O. (2005). Zebrafish Gli3 functions as both an activator and a repressor in Hedgehog
830 signaling. Dev. Biol. *277*, 537–556.

831 Vanderlaan, G., Tyurina, O. V., Karlstrom, R.O., and Chandrasekhar, A. (2005). Gli function
832 is essential for motor neuron induction in zebrafish. Dev. Biol. *282*, 550–570.

833 Vierstra, J., Rynes, E., Sandstrom, R., Zhang, M., Canfield, T., Hansen, R.S., Stehling-Sun,
834 S., Sabo, P.J., Byron, R., Humbert, R., et al. (2014). Mouse regulatory DNA landscapes
835 reveal global principles of cis-regulatory evolution. Science *346*, 1007–1012.

836 Waddington, C.H. (1942). Canalization of development and the inheritance of acquired
837 characters. Nature *150*, 563–565.

838 Waddington, C.H. (1957). The strategy of the genes (George Allen & Unwin Ltd).

839 Wang, H., Lei, Q., Oosterveen, T., Ericson, J., and Matise, M.P. (2011). Tcf/lef repressors
840 differentially regulate shh-gli target gene activation thresholds to generate progenitor
841 patterning in the developing CNS. Development *138*, 3711–3721.

842 Wang, X., Zhao, Z., Muller, J., Iyu, A., Khng, A.J., Guccione, E., Ruan, Y., and Ingham,
843 P.W. (2013). Targeted inactivation and identification of targets of the Gli2a transcription
844 factor in the zebrafish. Biol. Open *2*, 1203–1213.

845 Wilson, S.I., Shafer, B., Lee, K.J., and Dodd, J. (2008). A Molecular Program for
846 Contralateral Trajectory: Rig-1 Control by LIM Homeodomain Transcription Factors.
847 Neuron *59*, 413–424.

848 Xiong, F., Tentner, A.R., Huang, P., Gelas, A., Mosaliganti, K.R., Souhait, L., Rannou, N.,

849 Swinburne, I.A., Obholzer, N.D., Cowgill, P.D., et al. (2013). Specified neural progenitors
850 sort to form sharp domains after noisy Shh signaling. Cell *153*, 550–561.
851 Zagorski, M., Tabata, Y., Brandenberg, N., Lutolf, M.P., Tkačik, G., Bollenbach, T., Briscoe,
852 J., and Kicheva, A. (2017). Decoding of position in the developing neural tube from
853 antiparallel morphogen gradients. Science *356*, 1379–1383.
854 Zhang, Y., Narayan, S., Geiman, E., Lanuza, G.M., Velasquez, T., Shanks, B., Akay, T.,
855 Dyck, J., Pearson, K., Gosgnach, S., et al. (2008). V3 Spinal Neurons Establish a Robust and
856 Balanced Locomotor Rhythm during Walking. Neuron *60*, 84–96.
857

858 Fig.1

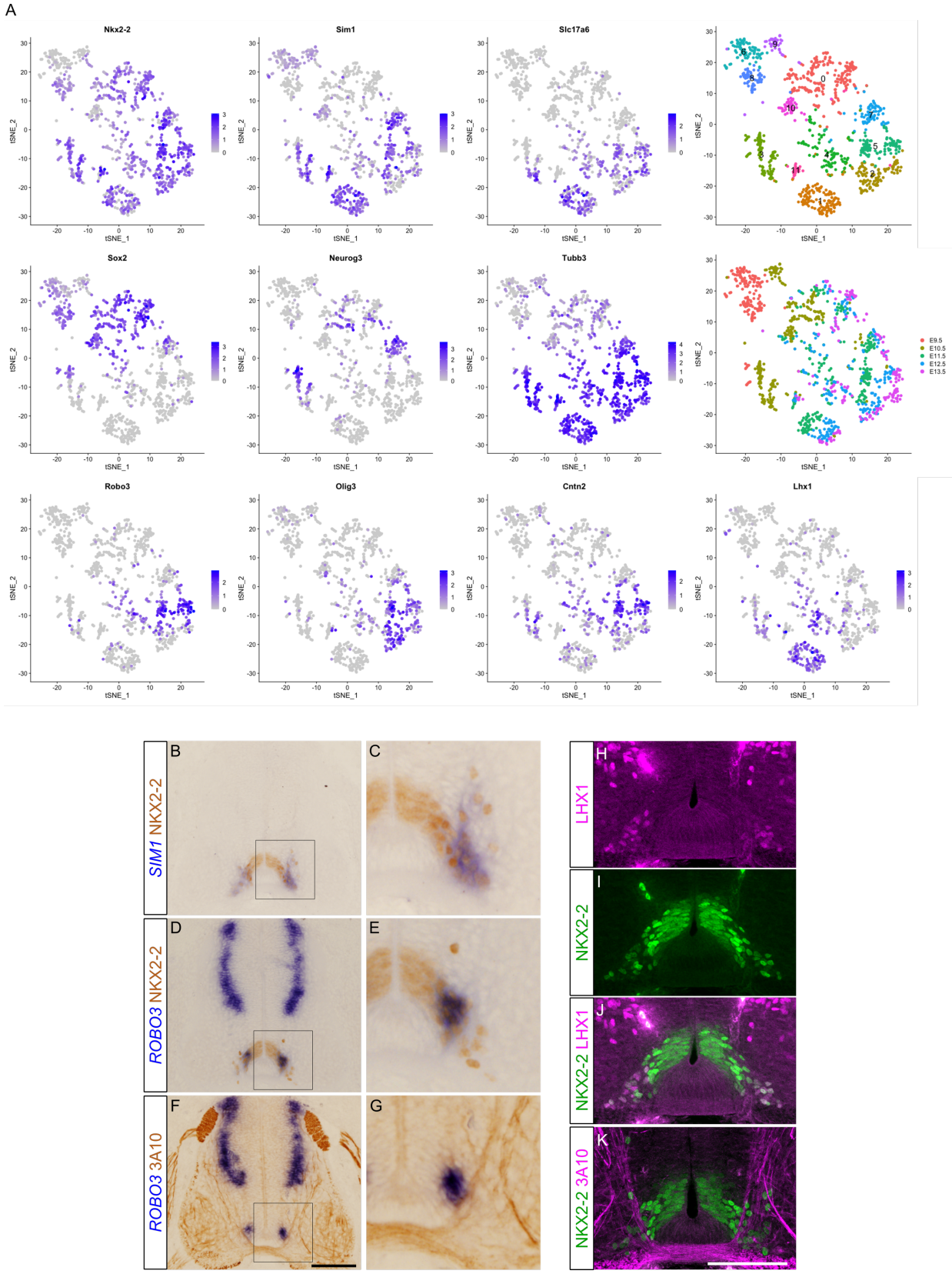
A
Nkx2-2
Sim1
Slc17a6
Sox2
Neurog3
Tubb3
Robo3
Olig3
Cntn2
Lhx1
tSNE_1
tSNE_2
E9.5
E10.5
E11.5
E12.5
E13.5
B
C
D
E
F
G
H
I
J
K
SIM1 NKX2-2
ROBO3 NKX2-2
ROBO3 3A10
LHX1
NKX2-2
NKX2-2 LHX1
NKX2-2 3A10

859

Fig.2

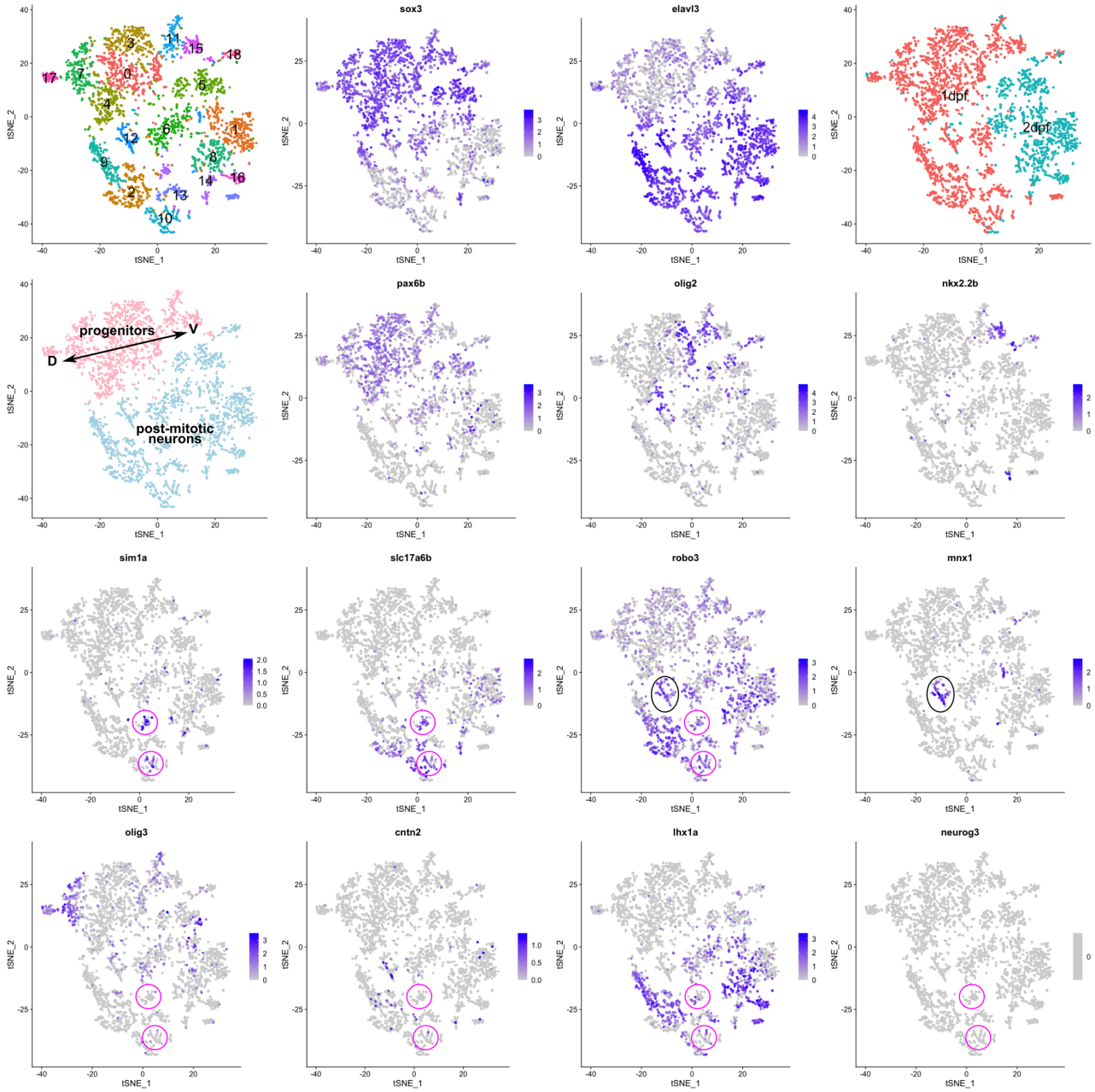
sox3
elavl3
1dpf
2dpf
progenitors
V
D
post-mitotic neurons
pax6b
olig2
nkx2.2b
sim1a
slc17a6b
robo3
mnx1
olig3
cntn2
lhx1a
neurog3
tSNE_1
tSNE_2

862 Fig.3

863

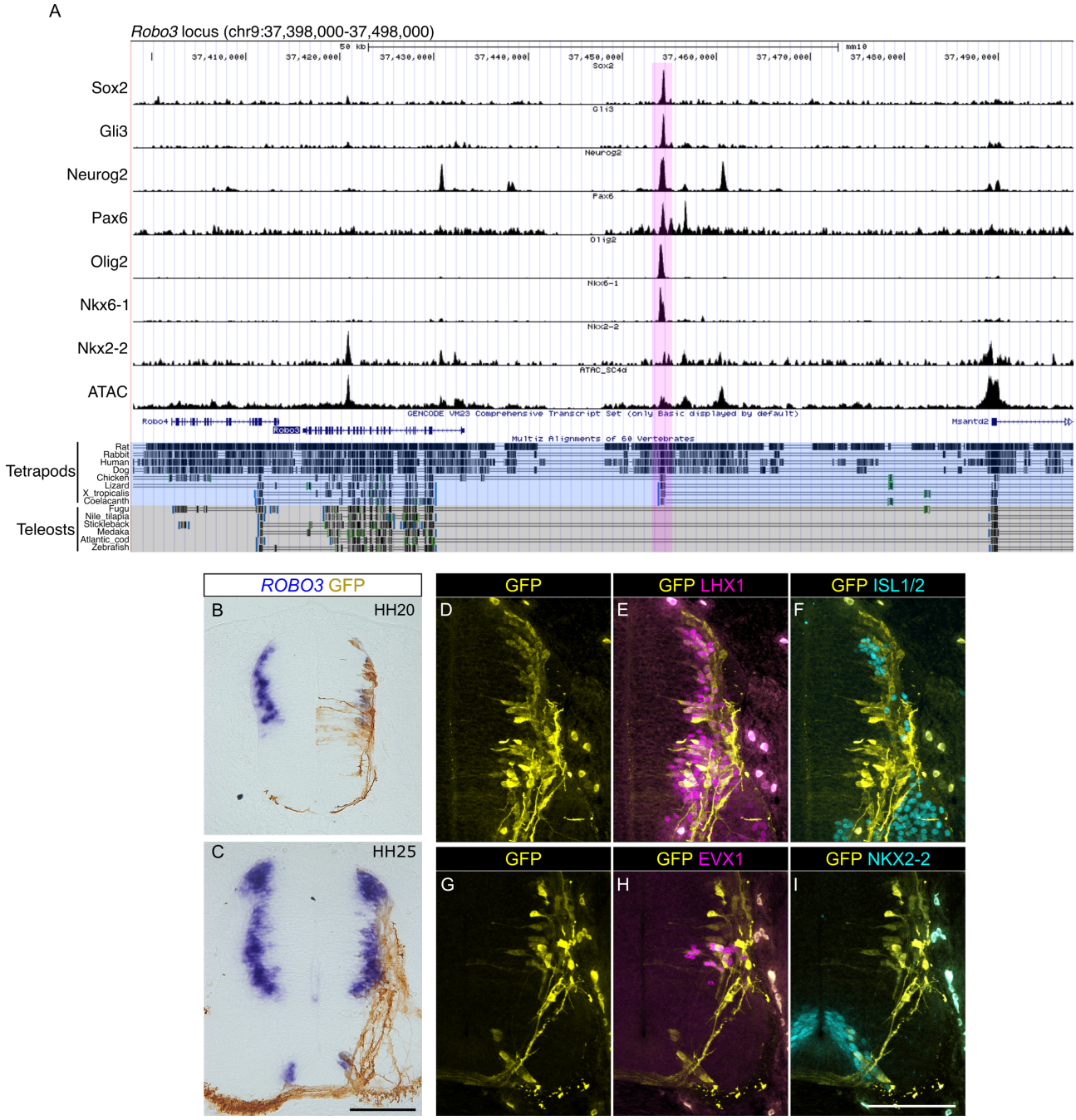
A
Robo3 locus (chr9:37,398,000-37,498,000)
Sox2
Gli3
Neurog2
Pax6
Olig2
Nkx6-1
Nkx2-2
ATAC
Tetrapods
Teleosts
ROBO3 GFP
B
HH20
C
HH25
GFP
GFP LHX1
GFP ISL1/2
D
E
F
GFP
GFP EVX1
GFP NKX2-2
G
H
I

Fig.4

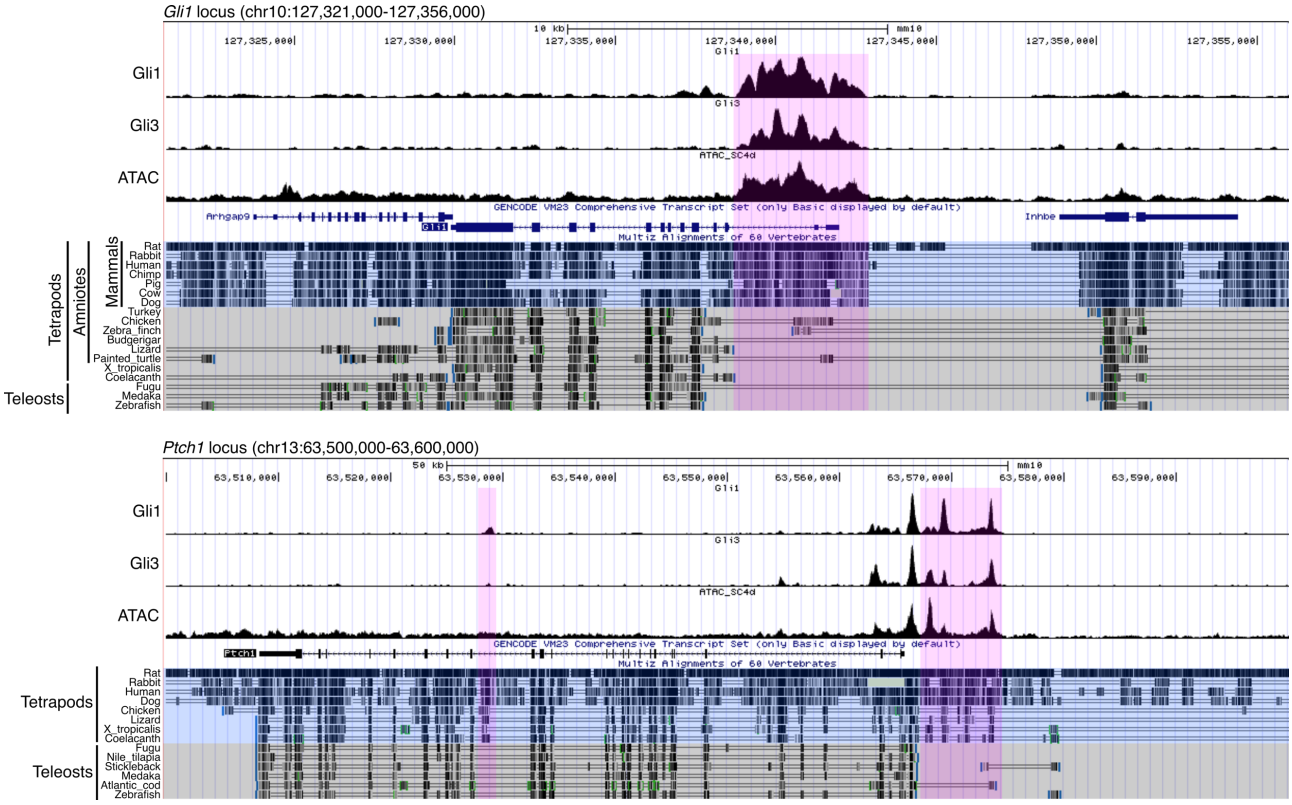
Gli1 locus (chr10:127,321,000-127,356,000)
Gli1
Gli3
ATAC
GENCODE VM23 Comprehensive Transcript Set (only Basic displayed by default)
Multiz Alignments of 60 Vertebrates
Tetrapods
Amniotes
Mammals
Teleosts
Rat
Rabbit
Human
Chimp
Pig
Cow
Dog
Turkey
Chicken
Zebra_finch
Budgerigar
Lizard
Painted_turtle
X_tropicalis
Coelacanth
Fugu
Medaka
Zebrafish
Ptch1 locus (chr13:63,500,000-63,600,000)
Gli1
Gli3
ATAC
GENCODE VM23 Comprehensive Transcript Set (only Basic displayed by default)
Multiz Alignments of 60 Vertebrates
Tetrapods
Teleosts
Rat
Rabbit
Human
Dog
Chicken
Lizard
X_tropicalis
Coelacanth
Fugu
Nile_tilapia
Stickleback
Medaka
Atlantic_cod
Zebrafish

866 Fig.5

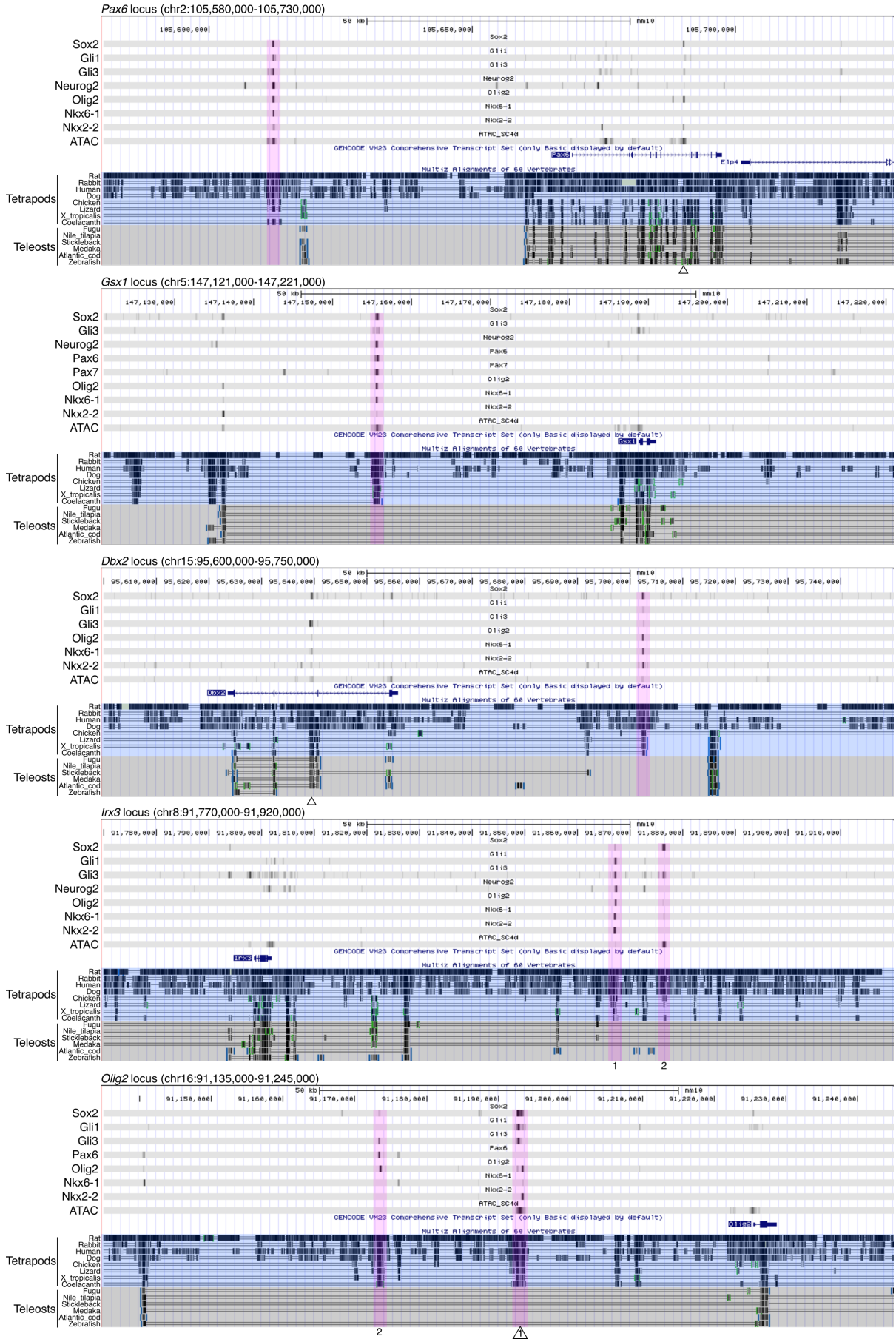
Pax6 locus (chr2:105,580,000-105,730,000)
Gsx1 locus (chr5:147,121,000-147,221,000)
Dbx2 locus (chr15:95,600,000-95,750,000)
Irx3 locus (chr8:91,770,000-91,920,000)
Olig2 locus (chr16:91,135,000-91,245,000)
Sox2
Gli1
Gli3
Neurog2
Olig2
Nkx6-1
Nkx2-2
ATAC
Pax6
Pax7
GENCODE VM23 Comprehensive Transcript Set (only Basic displayed by default)
Multiz Alignments of 60 Vertebrates
Tetrapods
Teleosts
Rat
Rabbit
Human
Dog
Chicken
Lizard
X_tropicalis
Coelacanth
Fugu
Nile_tilapia
Stickleback
Medaka
Atlantic_cod
Zebrafish
1
2

867 Fig.6

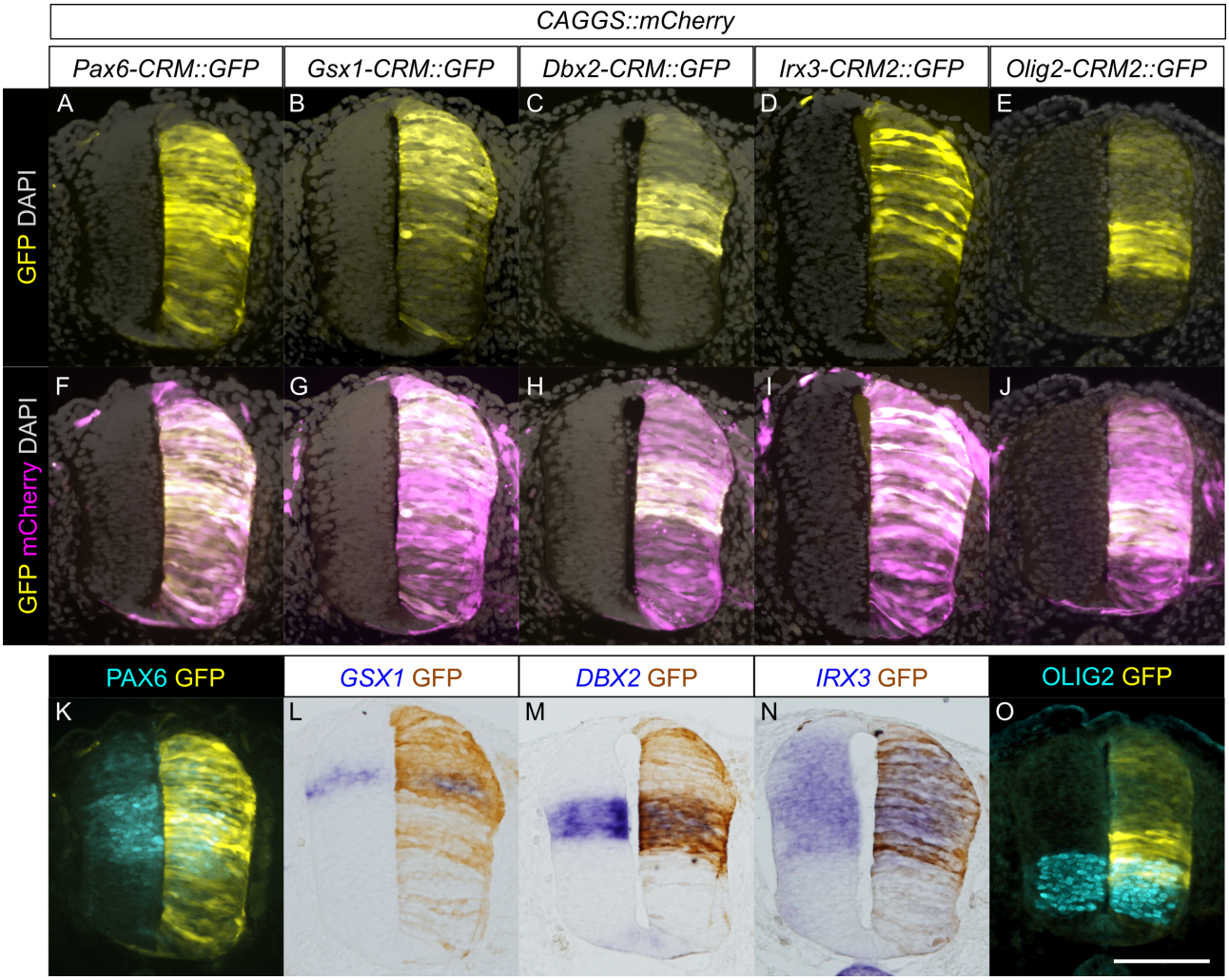
CAGGS::mCherry
Pax6-CRM::GFP
Gsx1-CRM::GFP
Dbx2-CRM::GFP
Irx3-CRM2::GFP
Olig2-CRM2::GFP
GFP DAPI
GFP mCherry DAPI
A
B
C
D
E
F
G
H
I
J
PAX6 GFP
GSX1 GFP
DBX2 GFP
IRX3 GFP
OLIG2 GFP
K
L
M
N
O

868 Fig.7

869

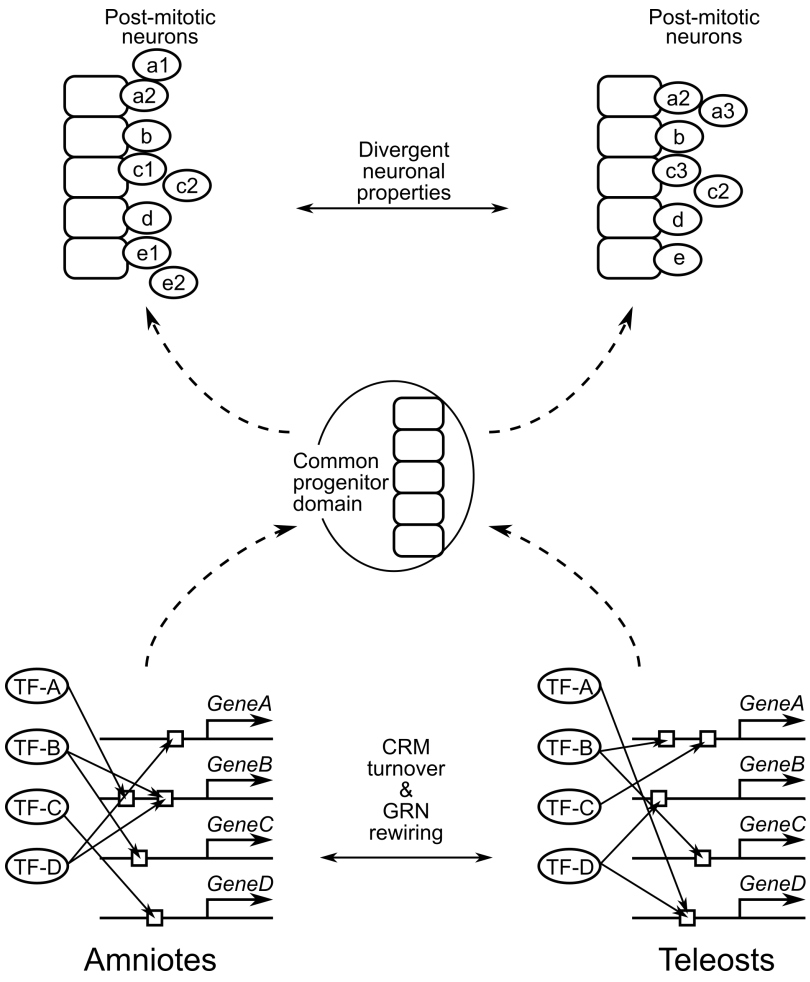
Post-mitotic neurons
a1
a2
b
c1
c2
d
e1
e2
Divergent neuronal properties
Post-mitotic neurons
a2
a3
b
c3
c2
d
e
Common progenitor domain
TF-A
TF-B
TF-C
TF-D
GeneA
GeneB
GeneC
GeneD
CRM turnover & GRN rewiring
TF-A
TF-B
TF-C
TF-D
GeneA
GeneB
GeneC
GeneD
Amniotes
Teleosts